PAPER • OPEN ACCESS

Three-dimensional single-particle tracking in live cells: news from the third dimension

To cite this article: A Dupont *et al* 2013 *New J. Phys.* **15** 075008

View the article online for updates and enhancements.

Three-dimensional single-particle tracking in live cells: news from the third dimension

A Dupont[1], M Gorelashvili[2], V Schüller[2], F Wehnekamp[1], D Arcizet[2], Y Katayama[1], D C Lamb[1,3,5] and D Heinrich[2,4,5]

[1] Department of Chemistry, Center for NanoScience and Center for Integrated Protein Science, Munich, Ludwig-Maximilians-Universität München, Butenandtstrasse 5-13, D-81377 München, Germany
[2] Faculty of Physics and Center for Nanoscience, Ludwig-Maximilians-Universität München, Geschwister-Scholl-Platz 1, D-80539 München, Germany
[3] Department of Physics, University of Illinois at Urbana-Champaign, Urbana, IL 61820, USA
[4] Leiden Institute of Physics, LION, Leiden University, Niels Bohrweg 2, 2333-CA Leiden, The Netherlands
E-mail: heinrich@physics.leidenuniv.nl and d.lamb@lmu.de

Abstract. Single-particle tracking (SPT) is of growing importance in the biophysical community. It is used to investigate processes such as drug and gene delivery, viral uptake, intracellular trafficking or membrane-bound protein mobility. Traditionally, SPT is performed in two dimensions (2D) because of its technical simplicity. However, life occurs in three dimensions (3D) and many methods have been recently developed to track particles in 3D. Now, is the third dimension worth the effort? Here we investigate the differences between the 2D and 3D analyses of intracellular transport with the 3D development of a time-resolved mean square displacement (MSD) analysis introduced previously. The 3D trajectories, and the 2D projections, of fluorescent nanoparticles were obtained with an orbital tracking microscope in two different cell types: in *Dictyostelium discoideum* ameba and in adherent, more flattened HuH-7

[5] Authors to whom any correspondence should be addressed.

human cells. As expected from the different 3D organization of both cells' cytoskeletons, a third of the active transport was lost upon projection in the ameba whereas the identification of the active phases was barely affected in the HuH-7 cells. In both cell types, we found intracellular diffusion to be anisotropic and the diffusion coefficient values derived from the 2D analysis were therefore biased.

S Online supplementary data available from stacks.iop.org/NJP/15/075008/mmedia

Contents

1. Introduction

The tracking of individual particles as they go about performing their function can provide quantitative mechanistic information that is unattainable in classical ensemble methods. Thus, the particle's motion can be quantitatively analyzed in terms of diffusion coefficient [1], instantaneous velocity [2], step size [3] or local extent of confinement [4]. Such features may reveal the interactions of the tracked particle with its local surroundings [5] as well as the local substructure of its micro-environment [6, 7]. Single-particle tracking (SPT) in living cells was first accomplished on proteins diffusing in the cell membrane [8, 9] where the diffusion is purely two dimensional (2D). In that case, as well as in isotropic systems, the tracking in two dimensions is sufficient to obtain accurate results. But inside cells, the real motion occurs in three dimensions (3D). In the second case or in any anisotropic medium, if the tracking

is achieved in 2D, a part of the information contained in the real trajectory is missing in the analysis of the 2D projected trajectory. The analysis could therefore lead to misevaluation of the motion parameters such as the diffusion coefficient or the velocity. Although the technical advances of SPT have generated an increasing demand for such techniques to follow single biomolecules in living cells, these effects have not been experimentally addressed yet and are still to be quantified. Within the last decade, a new generation of 3D tracking methods has been established that makes it possible to track single particles in 3D with high temporal and spatial resolution [10–13]). This new class of methods allows the tracking of single biomolecules in 3D in living cells but they are more difficult to perform than 2D imaging and tracking. Is the effort required to obtain the third dimension worth it and does it bring valuable information that is unattainable by 2D tracking? To tackle this question for intracellular transport, we tracked fluorescent nanoparticles in living cells using a home-made orbital tracking microscope capable of tracking particles in 3D in real time with a high spatial resolution [12, 14].

In addition to the advances in acquisition of trajectories using SPT, more elaborate methods have been developed to analyze the data. One approach by Bouzigues and Dahan [15] used the correlation of the instantaneous velocity to recognize directed motion in living cells. This method was adapted for 3D analysis by the group of Moerner [16] and used to investigate the motion of mRNA in yeast. Another elegant approach was discussed by Yang where a maximum likelihood method was used to recognize changes in diffusion coefficients within a trajectory [17]. We have applied the time-resolved TRAnSpORT algorithm described previously [18] and have adapted it for tracking in 3D. The nanoparticles were tracked in two different cell types having different 3D aspect ratios: 3D *Dictyostelium discoideum* and quasi-2D HuH-7 human cells. We compared the same data with and without the third dimension. In the case of 2D imaging and tracking, only trajectories contained in the thin observation volume are selected whereas what would be less out-of-plane trajectories in 2D are still considered in our analyses and compared. Based on a local mean-square-displacement (MSD) analysis, the TRAnSpORT algorithm, modified to perform the analysis in 3D, dissects a trajectory into different transport events identified as active or passive phases. The distribution of these phases was calculated with the 2D and the 3D analyses as well as the diffusion coefficients of passive phases and the velocity of active phases. By comparing these results, we show that intracellular diffusion is not purely isotropic and that 2D trajectories cannot be simply scaled up to 3D. The estimation of the diffusion coefficient was more strongly biased in the HuH-7 cells whereas the active transport analysis in these quasi-2D cells was only barely affected by the projection. In contrast, a third of the active phases in the roundish ameba cells were wrongly assigned to passive phases in the 2D analysis, revealing the quasi-isotropic organization of the cell's cytoskeleton. Hence, for an accurate determination of the diffusion coefficient and characterization of the different dynamic phases, a 3D tracking and analysis is required. Here, we measured and quantified the effect of reducing a 3D intracellular motion to its 2D projection.

2. Theory

2.1. Extension of the time-resolved mean square displacement analysis to three dimensions (3D)

Previously, we described a rolling-average algorithm able to reliably separate periods of active and passive motion from 2D trajectories of particles in live cells [18]. This approach is based on

the analysis of the MSD and the directional persistence from an analysis of the angle between steps. In short, a local MSD analysis is calculated in a rolling window of duration T along the trajectory and, for every time point t, the corresponding local MSD plot is fitted to a power law:

$$\langle \Delta R_{nD}^2(\delta t) \rangle = \left\langle \left(\vec{R}(t + \delta t) - \vec{R}(t) \right)^2 \right\rangle_{t-T/2 < t < t+T/2} = An\delta t^\alpha, \tag{1}$$

where n is the number of dimensions. This local MSD analysis and choices of rolling window size were investigated theoretically in [19]. When the particle is transported by molecular motors along the microtubules or the actin filaments, the motion is referred to as active. Otherwise the transport mode is defined as passive (intracellular diffusion). Further, we subdivide the passive motion mode into diffusive and subdiffusive. The value of the α-exponent together with the trajectory's angle deviation $\Delta\Phi$ are used to classify a local trajectory into

  (i) active motion when $\alpha = 2 \pm \sigma_\alpha$ and $\Delta\Phi = 0 \pm \sigma_\Phi$,
 (ii) diffusive motion when $\alpha = 1 \pm \sigma_\alpha$,
(iii) or subdiffusive motion when $\alpha < 1 - \sigma_\alpha$,

with $\sigma_\alpha = 0.3$ and $\sigma_\phi = 0.9$ rad. These conditions are smoothed so that no isolated data point is categorized as a different phase than the surrounding points. From the analysis, the distributions of the α-exponents, of the velocities during active transport, and of the diffusion coefficients during passive phases as well as the proportion of active, diffusive and subdiffusive states are obtained.

For Brownian motion in an isotropic medium, the MSD is given by

$$\langle \Delta R_{nD}^2(\delta t) \rangle = 2nD\delta t, \tag{2}$$

where D is the diffusion coefficient. Within the complex environment of the cell, random motion is often hindered or enhanced by obstacles and anomalous diffusion is observed. In this case, the MSD can be written as

$$\langle \Delta R_{nD}^2(\delta t) \rangle = 2nD\delta t^\alpha, \tag{3}$$

where α is the anomalous diffusion exponent with $\alpha < 1$ and D is a more general pseudo-diffusion coefficient. It reflects the amount of hindrance or enhancement to Brownian diffusion (which corresponds to $\alpha = 1$). For isotropic motion, a one-dimensional, 2D or 3D analysis will yield the same diffusion coefficient. In this case, the advantage of 3D tracking is the fact that the particle can be followed for a longer period of time than in conventional wide-field microscopy as tracking is not limited to a single focal plane.

For active transport, the MSD is given by

$$\langle \Delta R_{nD}^2(\delta t) \rangle = (v\delta t)^2 + 2nD\delta t^\alpha, \tag{4}$$

where v is the velocity of transport. Random diffusion is typically negligible during transport due to the physical link of the cargo to the cytoskeleton via motor proteins and the second term can then be ignored. These two types of motions can be combined into a single model:

$$\langle \Delta R_{nD}^2(\delta t) \rangle = An\delta t^\alpha, \tag{5}$$

where the exponent $\alpha < 1$ for subdiffusion, ~ 1 for random diffusion, $1 < \alpha < 2$ for super-diffusion and ~ 2 for active transport. For diffusion in general, $A = 2D$, and for active transport, $nA = v^2$. In particular, for 2D and 3D, the MSD reads as follows:

$$\langle \Delta R_{2D}^2(\delta t) \rangle = \langle \Delta x^2 + \Delta y^2 \rangle = 2A\delta t^\alpha, \tag{6}$$

$$\left\langle \Delta R_{3D}^2(\delta t)\right\rangle = \left\langle \Delta x^2 + \Delta y^2 + \Delta z^2\right\rangle = 3A\delta t^\alpha = \tfrac{3}{2}\left\langle \Delta R_{2D}^2(\delta t)\right\rangle. \tag{7}$$

The exponent should have the same value regardless of whether it is calculated from a 2D projection or from the 3D trajectory. Hence, the proper analysis of a 2D projection of a random trajectory is sufficient for determining the diffusion coefficient when the motion is purely random or isotropic. In contrast, when a particle is undergoing active transport, the velocities obtained from 2D projections and 3D trajectories will differ on average by $\sqrt{2/3} \approx 0.82$. If the system is not purely isotropic, these relations will change. Here, we quantify these ratios in two different cell types having different 3D geometries and cytoskeleton properties.

3. Materials and methods

3.1. Simulation of 3D Brownian motion

A trajectory of a particle undergoing Brownian motion was simulated over 35 000 steps. For each step, the motion of the particle was determined individually for each dimension. The distances were determined randomly from a normal distribution with a variance of 102 nm and added to the current position of the particle to determine the new position. The time interval was set to 32 ms between steps to mimic the experimental data, which yields an average diffusion coefficient of $0.163 \, \mu\mathrm{m}^2 \, \mathrm{s}^{-1}$ for the simulation.

3.2. 3D tracking

A custom-built microscope system was constructed around a Zeiss Axiovert 200 inverted microscope base. A Nikon water immersion objective (NA 1.20, magnification $63\times$) was mounted on a piezo-objective positioner (MIPOS 100PL CAP, Piezosystem Jena). An x–y–z piezo-stage (P-517.3CL, PhysikInstrumente) was used for calibration. The orbital tracking was controlled with SimFCS (Globals Software), and the piezo-stage was controlled with Labview (National Instruments). This system allowed real-time tracking simultaneously with wide-field fluorescence imaging. Further details are given elsewhere [14].

3.3. Trajectory analysis with the TRAnSpORT algorithm

A sliding window was used to calculate MSD plots along a trajectory to recognize different types of motional behavior within the same trajectory. The window size for analysis was 60 data points, each obtained with a time resolution of 32 ms, yielding a total duration of $T = 1.92$ s. For analysis purposes, the MSD was only calculated and fitted up to one fourth of the length of the local MSD window for different lag times between $\delta t = 0.032$ and 0.480 s. The errors on average diffusion coefficients and average α-exponents are the standard deviation of the mean for simulations and *in vitro* experiments. Due to the running average, we only considered non-overlapping intervals as statistically independent. To allow a detailed comparison of the asymmetric distributions determined from the live-cell measurements, we chose to fit the distributions to empirically chosen functions (lognormal and β distributions) and compared the peak values obtained. The errors are given by the uncertainty in determination of the peak position of the distribution. In addition, the complete results from all the fits are given in supplementary material (available from stacks.iop.org/NJP/15/075008/mmedia) and the corresponding average values are given in table 1.

Table 1. Summary table of the results obtained from the 3D and 2D analyses of nanoparticle trajectories obtained in *Dictyostelium discoideum* cells and HuH-7 cells. The fit parameters are given in the supplementary material (available from stacks.iop.org/NJP/15/075008/mmedia).

	D. discoideum			HuH-7		
	3D	2D-*xy*	2D/3D	3D	2D-*xy*	2D/3D
D_{peak} (μm^2 s^{-1})	0.0055	0.0037	0.67	0.0032	0.0010	0.31
Average	0.0088	0.0054	0.61	0.0066	0.0020	0.30
V_{active} (μms^{-1})	0.58	0.42	0.72	0.56	0.40	0.71
Average	0.69	0.52	0.75	0.78	0.67	0.86
Exponent α_{peak}	1.65	1.63	0.99	0.81	0.58	0.72
Average	1.54	1.48	0.96	0.98	0.91	0.93
MSD (μm^2)	4.91×10^{-4}	2.95×10^{-4}	0.60	4.72×10^{-4}	3.03×10^{-4}	0.64
Active states	38%	27%	0.71	6%	7%	1.27
Diffusive states	22%	32%	1.45	69%	48%	0.69
Subdiffusive states	0.1%	0.6%	[a]	16%	34%	2.13

[a] The ratio is not statistically significant.

3.4. Two-dimensional analysis

The 2D trajectory was determined by projecting the actual 3D trajectory on a 2D plane. In other words, only the *x*–*y* coordinates were used for the analysis. Real 2D tracking leads to shorter and less precise tracks that are contained in the focal plane. By using the 2D projections of the 3D tracks, we obtained longer tracks and we ensured that the *z* position of the particle has no influence on the tracking accuracy. In addition, the trajectories with large movement in *z* were taken into account whereas they would not be observable in traditional 2D tracking. Hence, the 2D analysis was achieved on all possible 2D trajectories without restriction and in this way we compared data coming from the same particles, with no other source of differences than the 3D versus 2D.

3.5. Beads in a glucose–water solution

To verify that the orbital tracking system does not introduce any anisotropic artifact, polymer microbeads (190 nm Spherotech Ultra Rainbow) were tracked in 3D in a glucose–water solution (50% v/v). The data from 30 individual bead trajectories were merged, giving a virtual total trajectory of 20 500 data points. A classical mean-square-displacement analysis was performed on the projections of this total trajectory on the *x*–*y*, *x*–*z* and *y*–*z* planes. As observed during these control experiments, the tracking of purely diffusive particles in solution with better than 10 nm accuracy is sensitive to mechanical drift due to temperature instabilities in the laboratory. Hence, care was taken to ensure that the room temperature was constant during the measurement.

3.6. Nanoparticles in Dictyostelium discoideum GFP-α-tubulin

The nanoparticles consisted of polyplexes freshly prepared as described previously [20] and incubated at room temperature for 30 min before each experiment. They consisted of 40 base pairs DNA labeled with two fluorescent dyes ATTO 647N and ATTO 565 (ATTO Tec GmbH,

Germany) and a mixture of LPEI (22 kDa)–PEG (20 kDa) and LPEI (22 kDa) polymers. The polyplex particles had an average hydrodynamic radius of 200 nm. *D. discoideum* GFP-α-tubulin strains HG1668 [21] were cultured in antibiotic-free AX2 growth medium 24 h before the experiment. The medium was then exchanged to a growth medium exhibiting lower fluorescence 5 h prior to seeding in eight-well Lab-Tek chamber slides (Nunc GmbH & Co. KG, Germany). Cell density was approximately 40%. The cells were allowed to adhere to the chamber for 10 min prior to washing with phosphate buffer. The 100 μl diluted particle suspensions in phosphate buffer were then added to the cells to yield a final concentration of 0.4 μg per well. Particle uptake was facilitated by the small volume of fluid in the chamber. The chamber was filled with an additional 200 μl of buffer to provide cells with sufficient fluid for the duration of the experiment.

3.7. Nanoparticles in HuH-7 cells

DNA plasmids were double labeled with Cy3 and Cy5 (Label IT Kits, MIRUS) and DNA/polyethylenimine polyplexes were prepared as previously described [22]. The PEI–PEG polymers were modified with epidermal growth factor (EGF) to enhance the uptake efficiency and rate. The polyplexes were stored in aliquots at $-80\,°C$ until shortly before the measurements, at which time they were first warmed in a heat bath at $36\,°C$ and then added to cell culture medium at $37\,°C$. Experiments were started immediately after addition of the polyplexes and were performed for 3–4 h. The median particle size determined from similar preparations using dynamic light scattering was 266 ± 22 nm. These particles were tracked in HuH-7 human hepatome cells expressing eGFP-tubulin. For microscopy, the cells were grown in a NUNC chamber and kept for 1–2 days in an incubator ($37\,°C$ and 5% CO_2 atmosphere) before the experiment. Immediately before the measurements, the medium was exchanged with CO_2 independent medium and mounted onto a microscope heat chamber (Temp-Control 37-2 digital). We did not use an objective heater as evaporation of the water immersion fluid negatively influenced our experiments.

4. Results

4.1. Simulation

To test the validity of the analysis method, 3D Brownian diffusion of particles with a diffusion coefficient of $0.163\ \mu m^2\,s^{-1}$ was simulated (see Materials and methods) and the 3D particle trajectories and their 2D projections were evaluated by a global MSD analysis and by the local MSD algorithm TRAnSpORT [18]. To obtain reliable error bars in the global MSD analysis, the trajectory was cut into 15 segments, which were individually analyzed by fitting their MSD to obtain the α-exponent and the diffusion coefficient. The results from a 3D analysis ($\alpha_{3D} = 1.02 \pm 0.04$ and $D_{3D} = 0.16 \pm 0.01\ \mu m^2\,s^{-1}$) and from analysis on the 2D x–y projection ($\alpha_{2D} = 0.99 \pm 0.05$ and $D_{2D} = 0.16 \pm 0.01\ \mu m^2\,s^{-1}$) are in agreement with each other and with the expected values within the errors ($\alpha_{th} = 1$). From the TRAnSpORT analysis, we extracted average α values of $\alpha_{3D}^{avg} = 1.04 \pm 0.01$ and $\alpha_{2Dproj}^{avg} = 1.01 \pm 0.01$ and average diffusion coefficients of $D_{3D}^{avg} = 0.149 \pm 0.002\ \mu m^2\,s^{-1}$ and $D_{2Dproj}^{avg} = 0.152 \pm 0.003\ \mu m^2\,s^{-1}$. The values for both α and D are consistent with each other within the error bars but differ slightly from the expected values. However, it should be kept in mind that the TRAnSpORT algorithm has been created to identify changes in diffusional behavior between active and

passive phases with a good time resolution. For high time resolution, a small MSD window is analyzed at the cost of absolute accuracy. Typically, α tends to be over-estimated and D under-estimated. Since the diffusion coefficient and the exponent are determined locally for each time point, the distribution can be plotted. To compare the results and extract the peak values of the distributions, the distributions were fitted to empirically chosen functions. The distributions of the α-exponent are fairly symmetric (figure 1(A)) with peak values ($\alpha_{3D}^{peak} = 1.04 \pm 0.01$ and $\alpha_{2Dproj}^{peak} = 1.02 \pm 0.01$) in the range of the average values obtained earlier. As expected, the distributions of the diffusion coefficient are asymmetric (figure 1(B)) [23]. The peak values ($D_{3D}^{peak} = 0.1259 \pm 5 \times 10^{-4}$ and $D_{2Dproj}^{peak} = 0.1258 \pm 6 \times 10^{-4} \, \mu m^2 \, s^{-1}$), therefore, differ from the average values but are consistent with each other within the calculated uncertainty. The small deviations observed show the uncertainties of the local MSD calculated on a finite time window and need to be considered when interpreting the results.

4.2. Isotropic 3D single-particle tracking

As a next step, the diffusion of fluorescent beads (190 nm Spherotech Ultra Rainbow) in a glucose–water mixture (50/50 v/v) was measured in real time and in 3D to test the isotropy of the experimental setup. For 3D SPT, an orbital tracking microscope with 32 ms temporal resolution and 10 nm spatial accuracy in all the three dimensions [12, 14] was used. All 20 500 data points from trajectories measured on a total of 30 particles (figure 1(C)) were concatenated into 15 fragments and analyzed independently to obtain a reliable error estimation. The 15 different MSDs were fit to a power law and the resulting exponents and diffusion coefficients were averaged. The uncertainty was taken as the standard error of the mean over this sample of 15 values. The analysis was performed in 3D on the global 3D trajectory and in 2D on the three different 2D projections of the global trajectory (x–y, x–z and y–z). These four average MSD curves are plotted in figure 1(D). The 3D MSD and three different 2D MSD analyses yielded α-exponents of $\alpha_{3D} = 1.02 \pm 0.06$, $\alpha_{xy} = 1.03 \pm 0.06$, $\alpha_{xz} = 1.01 \pm 0.07$ and $\alpha_{yz} = 0.99 \pm 0.05$ and diffusion coefficients of $D_{3D} = 0.23 \pm 0.01 \, \mu m^2 \, s^{-1}$, $D_{xy} = 0.24 \pm 0.01 \, \mu m^2 \, s^{-1}$, $D_{xz} = 0.22 \pm 0.01 \, \mu m^2 \, s^{-1}$ and $D_{yz} = 0.23 \pm 0.02 \, \mu m^2 \, s^{-1}$. The MSD curves as well as the obtained parameters (α and D) of the three possible 2D projections agree within experimental error showing that the tracking setup does not introduce any anisotropic bias. The same data set was then analyzed with the TRAnSpORT algorithm. The average MSD exponents were $\alpha_{3D}^{avg} = 1.15 \pm 0.01$ and $\alpha_{2Dproj}^{avg} = 1.12 \pm 0.01$. For regions of the trajectory categorized as diffusive, the average diffusion coefficients of $D_{3D}^{avg} = 0.216 \pm 0.007 \, \mu m^2 \, s^{-1}$ and $D_{2Dproj}^{avg} = 0.214 \pm 0.008 \, \mu m^2 \, s^{-1}$ were determined. Again, the exponent is over-estimated and the diffusion coefficient is slightly under-estimated. With real data, the experimental uncertainty, which is reflected as an offset of the MSD plot, leads to a further decrease in the accuracy of the TRAnSpORT algorithm as the effect of the experimental uncertainties is most prevalent at the short lag times of an MSD curve. In figures 1(E) and (F), we show the distributions of the MSD exponents and of the diffusion coefficients from the TRAnSpORT analysis as well as the fits used to obtain the peak values. The exponent has a symmetric distribution with a peak at $\alpha_{3D}^{peak} = 1.16 \pm 0.02$ and $\alpha_{2Dproj}^{peak} = 1.13 \pm 0.02$, respectively (figure 1(E)). Similar to the simulations above, the distribution of the diffusion coefficients is asymmetric with peak values of $D_{3D}^{peak} = 0.179 \pm 0.009 \, \mu m^2 \, s^{-1}$ and $D_{2Dproj}^{peak} = 0.183 \pm 0.009 \, \mu m^2 \, s^{-1}$ (figure 1(F)). Even though there are small deviations of the TRAnSpORT algorithm with respect to absolute values, the values determined for the 3D and 2D analyses are in agreement. Hence, the tracking
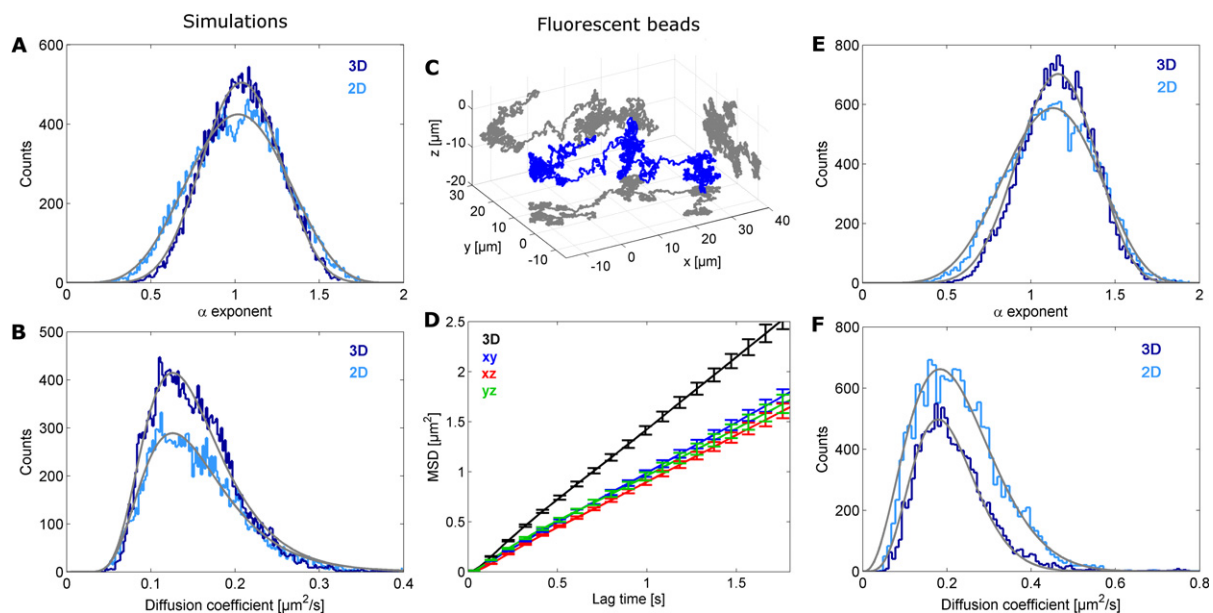
Figure 1. Verification of the algorithm and tracking setup using simulations and freely diffusing fluorescent beads. (A) Distributions of α-exponents obtained from the TRAnSpORT analysis of the simulated trajectory in 3D (dark blue) and in 2D (light blue). (B) Distributions of the diffusion coefficients obtained from the 3D (dark blue) and 2D (light blue) analyses of the same data set. The gray lines are fits to a modified β function (for α) and to a lognormal function (for D) to guide the eye and better extract the peak positions of the distributions. (C) The total 3D concatenated trajectory (20 500 data points, 660 s) resulting from the tracking of 30 individual fluorescent microspheres (190 nm) freely diffusing in a glucose–water solution (50% v/v). The 3D trajectory is shown along with the respective 2D projections in x–y, x–z and y–z. (D) The global 3D MSD (black) as well as the three different global 2D MSD plots, x–y (blue), x–z (red) and y–z (green), are shown. The MSD curves of the three possible 2D projections agree within experimental error, demonstrating the experimental accuracy and isotropy of the system. (E) Distributions of α-exponents obtained from the TRAnSpORT analysis in 3D (dark blue) and in 2D (light blue) of the trajectories from the fluorescent beads. (F) Distributions of the diffusion coefficients obtained from the 3D (dark blue) and 2D (light blue) analyses of the same data set. The gray lines are fits to a modified β function (for α and D) to guide the eye and better extract the peak positions.

system and the local MSD algorithm are well suited for investigating the effect of restricting the analysis of 3D trajectories in live cells to a 2D plane.

4.3. 3D tracking in D. discoideum cells

For the initial live-cell studies, we used *D. discoideum* cells, which we have investigated in detail using 2D tracking previously [24]. This ameba has a simple cytoskeleton without any

intermediate filaments or actin stress fibers. The cell shape is maintained by the microtubule network that creates tension between the nucleus and the cortex and has a rather isotropic structure. For convenience, we used cells with fluorescently labeled microtubules (GFP-α-tubulin). Fluorescent nanoparticles (polyplexes, see Materials and methods) were tracked in 3D with the orbital tracking microscope. The 3D trajectory and the respective 2D projection were analyzed with the time-resolved 3D and 2D algorithms, respectively. Figure 2 shows a representative trajectory and the corresponding 3D TRAnSpORT analysis. The wide-field image sequence in figure 2(A) shows an active transport phase along a microtubule between 12 and 15 s. The respective 3D trajectory and the corresponding 2D projections onto the x–y, x–z and y–z planes are shown in figure 2(B), z being the direction perpendicular to the coverslip. The particle undergoes phases of active transport (red) interrupted by phases of passive motion (blue). The results from the 3D time-resolved MSD analysis of this trajectory are shown in figures 2(C) and (D). In figure 2(C), all the local MSDs are displayed as a function of the trajectory time and the color represents the α-exponent determined from the fit. Figure 2(D) displays the total traveled distance, $R(t)$, of the tracked particle, the corresponding MSD-α value, the angle variation $\Delta\Phi$ between consecutive positions, the diffusion coefficient during passive transport phases and the instantaneous velocity (shown in gray) overlaid with the velocity determined from fits to the time-resolved MSD during phases of active transport (in red).

Twelve particles were tracked for a total of over 2200 s corresponding to a total of 70 238 data points. The results from the 3D and the 2D analyses derived from all *D. discoideum* data points are compared in figure 3. First of all, one notices that most of the peaks in the local MSDs plot (figure 3(A)) were strongly reduced when performing the analysis on the 2D projection. The ratio between the 2D and the 3D average MSD values was found to be 0.60, a value slightly lower than the expected value of 0.66 for isotropic Brownian motion. The distributions of the α-exponents obtained from the 2D and the 3D are shown in figure 3(B) (black) together with the sub-distributions for the active (red) and diffusive phases (blue). The average values are given in table 1. To estimate the peak values of the distribution, a modified β distribution (where the x-axis was expanded to run between 0 and 2 and values beyond 2 were ignored) was empirically chosen to fit the data (gray line). From the fits, peak α-exponents of $\alpha_{3D}^{peak} = 1.653 \pm 0.003$ and $\alpha_{2D}^{peak} = 1.632 \pm 0.004$ were determined ($\alpha_{3D}^{avg} = 1.543 \pm 0.007$ and $\alpha_{2D}^{avg} = 1.479 \pm 0.009$). As expected, the peak and average values of the α-exponent were barely affected by restriction of the trajectory to 2D although the distribution becomes broader towards lower values. The TRAnSpORT algorithm distinguishes between the phases of active transport and random diffusion and provides the distribution of the instantaneous velocities during the active phases (figure 3(C), dark red is the 3D analysis, light red is the 2D) and the distribution of the diffusion coefficients during the diffusive phases (figure 3(D), dark blue is the 3D analysis, light blue is the 2D). These distributions were fit to a modified β distribution and lognormal distributions, respectively, to extract the features from the data set (gray lines). The respective average values are given in table 1. A third of the phases recognized as active in the 3D analysis were assigned as passive phases in the 2D analysis (see table 1). This leads to the decrease in the amplitude of active events displayed in figure 3(C). The peak shifted from $0.582 \pm 0.004 \, \mu m \, s^{-1}$ in 3D to $0.416 \pm 0.003 \, \mu m \, s^{-1}$ in 2D, i.e. by a factor 0.72, whereas the expected ratio for isotropic motion is 0.82. The 2D velocity values are in agreement with previous studies which showed an average active velocity of $0.4 \, \mu m \, s^{-1}$ in *D. discoideum* cells with 2D image acquisition and tracking [18]. These misassignments were most probably due to phases of transport directed principally along the z-axis. This misinterpretation would be less prominent in conventional 2D
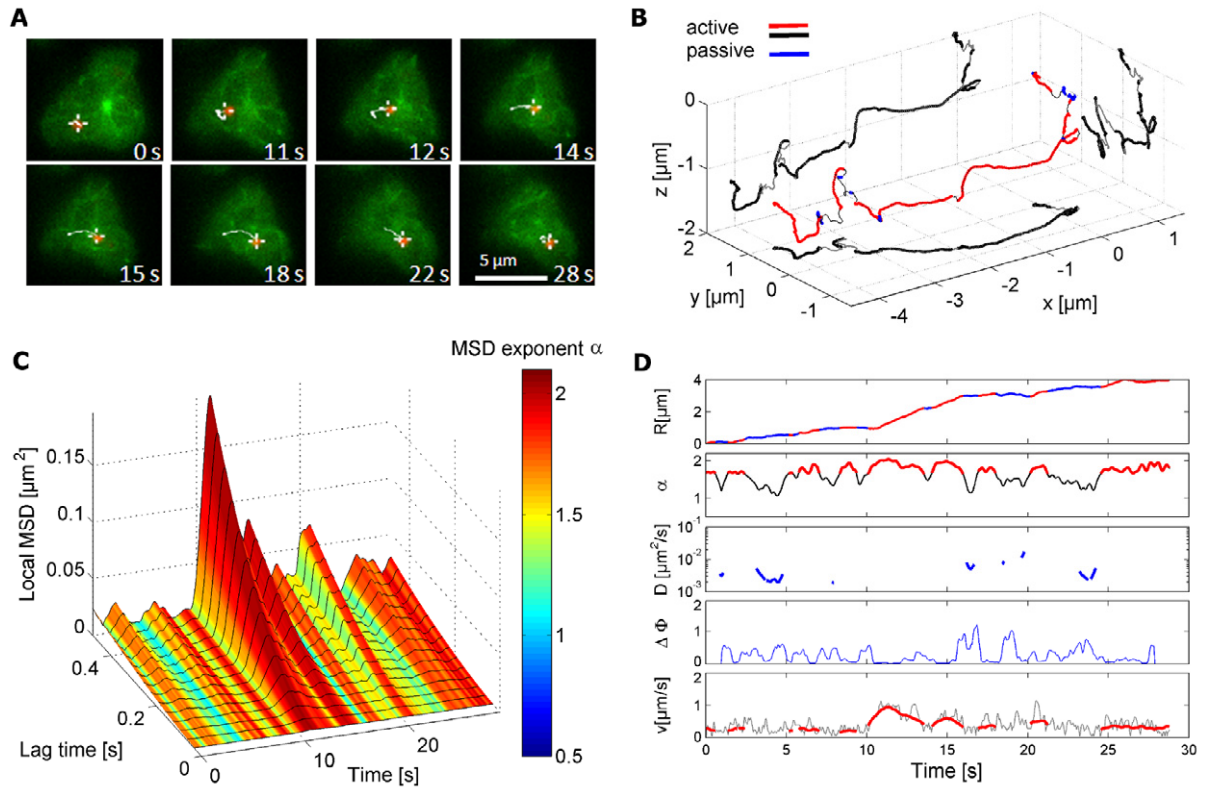
Figure 2. Tracking in *Dictyostelium discoideum* cells. (A) *D. discoideum-α*-tubulin cells (green) with endocytosed polyplexes (red). The white cross indicates the position of the particle and the white track shows the position during the preceding 2.5 s. The track shows a rapid movement over 4 μm between $t = 11$ and 14 s. (B) A three-dimensional representation of the particle's motion in the cell and associated projections of the trajectories in the *x–y*, *x–z* and *y–z* planes. The phases of active transport are shown in red and the diffusive phases are shown in blue. As seen in the projections, the polyplex moves significantly in the *z* direction. (C) The corresponding MSD plots obtained along the trajectory in a rolling window are shown in a 3D plot. The values of the α-exponents are encoded in color. Each value was determined by fitting the MSD function for every experimental time point *t*. (D) TRAnSpORT analysis results for this trajectory showing from top to bottom the absolute distance from the beginning of the trajectory, the exponent α, the average angle between consecutive steps $\Delta\Phi$, the diffusion coefficient for regions of diffusive motion and the velocity. Active transport is marked in red and regions of diffusive motion in blue. The values of active transport plotted in red in the lowest panel (i.e. graph of instantaneous velocity versus time) represent the velocity determined from the fit to the time-resolved MSD data.

wide-field microscopy where the particles that are transported in the *z*-direction quickly leave the focal plane and cannot be tracked further. The diffusion coefficient distributions also differ from 3D to 2D, with peak values of $D_{3D}^{peak} = (5.53 \pm 0.07) \times 10^{-3}$ and $D_{2D}^{peak} = (3.70 \pm 0.03) \times 10^{-3}$ ($D_{3D}^{avg} = (8.8 \pm 0.5) \times 10^{-3}$ and $D_{2D}^{avg} = (5.4 \pm 0.2) \times 10^{-3}$ μm^2 s^{-1}). For pure Brownian
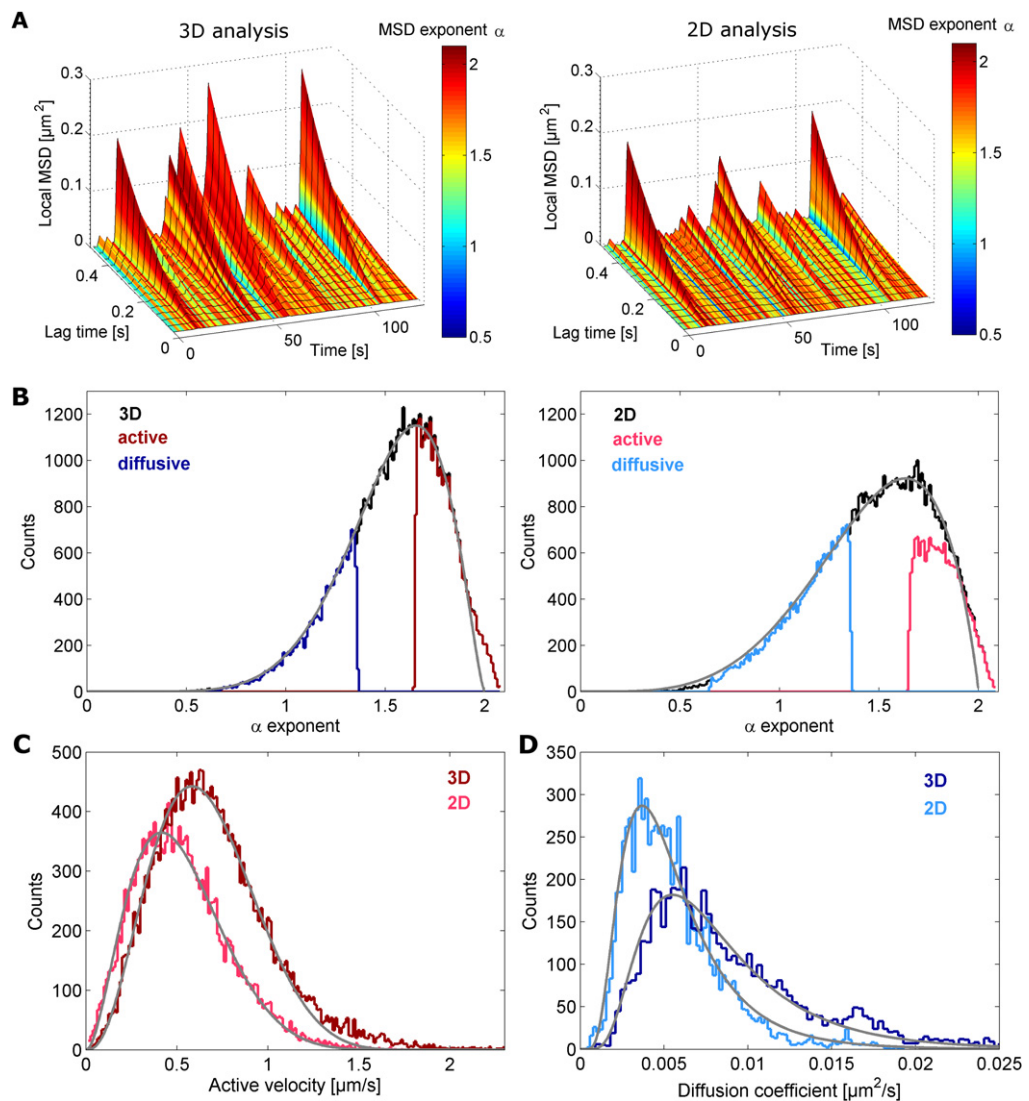
Figure 3. Comparison of the 3D and 2D *x–y* projection analyses in *D. discoideum* cells. (A) TRAnSpORT MSD plots from the 3D (left) and 2D (right) analyses of a nanoparticle moving within a *D. discoideum* cell. The $\langle R^2 \rangle$ values are significantly smaller in the 2D analysis than in the 3D analysis. (B) Distributions of α-exponents obtained from the fit of the 3D (left) and 2D (right) MSDs for every time point. The gray line is a fit to a modified β function to guide the eye and better extract the peak position. The distribution for active phases is shown in red and for passive phases in blue. (C) Distributions of active transport velocities from the 3D analysis (dark red) and the 2D *x–y* projection (light red). The distributions were fit to a modified β function to guide the eye and better extract the peak position for comparison (gray line). (D) The distributions of diffusion coefficients during passive phases in 3D (dark blue) and in 2D (light blue) are shown along with the respective fits to a lognormal distribution (gray line).

motion, the diffusion coefficient is expected to stay unchanged regardless of the dimensionality. We interpret the decrease in the diffusion coefficient by a factor of 0.67 from 3D to 2D as proof that the diffusion in *D. discoideum* living cells is not purely Brownian, whereas the loss of a third of active phases when analyzing in 2D only reveals that the active transport motion in *D. discoideum* is evenly distributed in all three directions.

4.4. 3D tracking in HuH-7 human cells

As a second cell line, we investigated the transport of polyplexes in HuH-7 cells as the majority of trafficking studies are performed on comparable quasi-two-dimensional, strongly adherent cell types. The cytoskeleton network of these planar cells is more complicated and more crowded than in *D. discoideum* cells as it contains actin stress fibers and intermediate filaments. Polyplexes were labeled with EGF to facilitate the uptake of these particles by the cells [20]). Five particles were tracked over a total of more than 2270 s corresponding to a total of 70 952 data points. The results from the 3D and 2D TRAnSpORT analyses are compared in figure 4 and the peak and average values are given in table 1. Unlike for the trajectories obtained in *D. discoideum*, the 2D local MSD plot derived from all HuH-7 data points retains all the features of the 3D MSD analysis (figure 4(A)). The movement was mainly diffusive with only short periods of active transport as determined from both analyses. For the HuH-7 cells, the 2D and 3D distributions of the α-exponents are clearly different (figure 4(B)) even though the average values remain similar. The peak values, obtained by fitting to a lognormal distribution, are $\alpha_{3D}^{peak} = 0.805 \pm 0.002$ and $\alpha_{2D}^{peak} = 0.575 \pm 0.004$, respectively, and differed by a factor of 0.72 whereas the average values are more similar ($\alpha_{3D}^{avg} = 0.98 \pm 0.01$ and $\alpha_{2D}^{avg} = 0.91 \pm 0.01$). Almost a quarter of the phases characterized as diffusive in the 3D analysis were recognized as subdiffusive in the 2D analysis, i.e. their exponent was reduced upon projection. Interestingly, the identification of the active phases was not affected by the projection (6% in 3D versus 7% in 2D, see table 1). Accordingly, the distributions of the active velocities found in 3D and in 2D are very similar (figure 4(C)). The peak shifted from $0.564 \pm 0.009\ \mu\mathrm{m\,s^{-1}}$ in 3D to $0.402 \pm 0.006\ \mu\mathrm{m\,s^{-1}}$, i.e. with a ratio of 0.71. This ratio needs to be considered carefully because the distributions were very noisy and the peak determination has relatively large uncertainties. In contrast, the distributions of the diffusion coefficients derived from the 2D and 3D analyses differed widely (figure 4(D)). The peak in the 2D distribution was much sharper and its value equaled only a third of the 3D peak diffusion coefficient ($D_{3D}^{peak} = (3.23 \pm 0.02)\ \times 10^{-3}$ and $D_{2D}^{peak} = (1.03 \pm 0.01) \times 10^{-3}\ \mu\mathrm{m^2\,s^{-1}}$, fitted to lognormal distribution). The same trend was observed in the average values ($D_{3D}^{avg} = (6.6 \pm 0.2) \times 10^{-3}$ and $D_{2D}^{avg} = (2.0 \pm 0.1) \times 10^{-3}\ \mu\mathrm{m^2\,s^{-1}}$). This strong reduction of the diffusion coefficient values taken together with the decrease in the α-exponents suggests that the diffusion in HuH-7 cells is (i) not Brownian and (ii) strongly anisotropic. In contrast, the active phase determination and characterization in HuH-7 cells was barely affected by the reduction to 2D, suggesting that the active transport occurs dominantly in a quasi-2D space, the plane of adherence.

5. Discussion

Motion in living cells is known to be complex, combining active transport phases with passive diffusion phases. Whereas restricting the analysis of a Brownian particle's trajectory to 2D has no influence on the results, the 2D analysis of a particle's trajectory in a living cell leads to bias and imprecision. In *D. discoideum* cells, where active transport was observed for 38% of
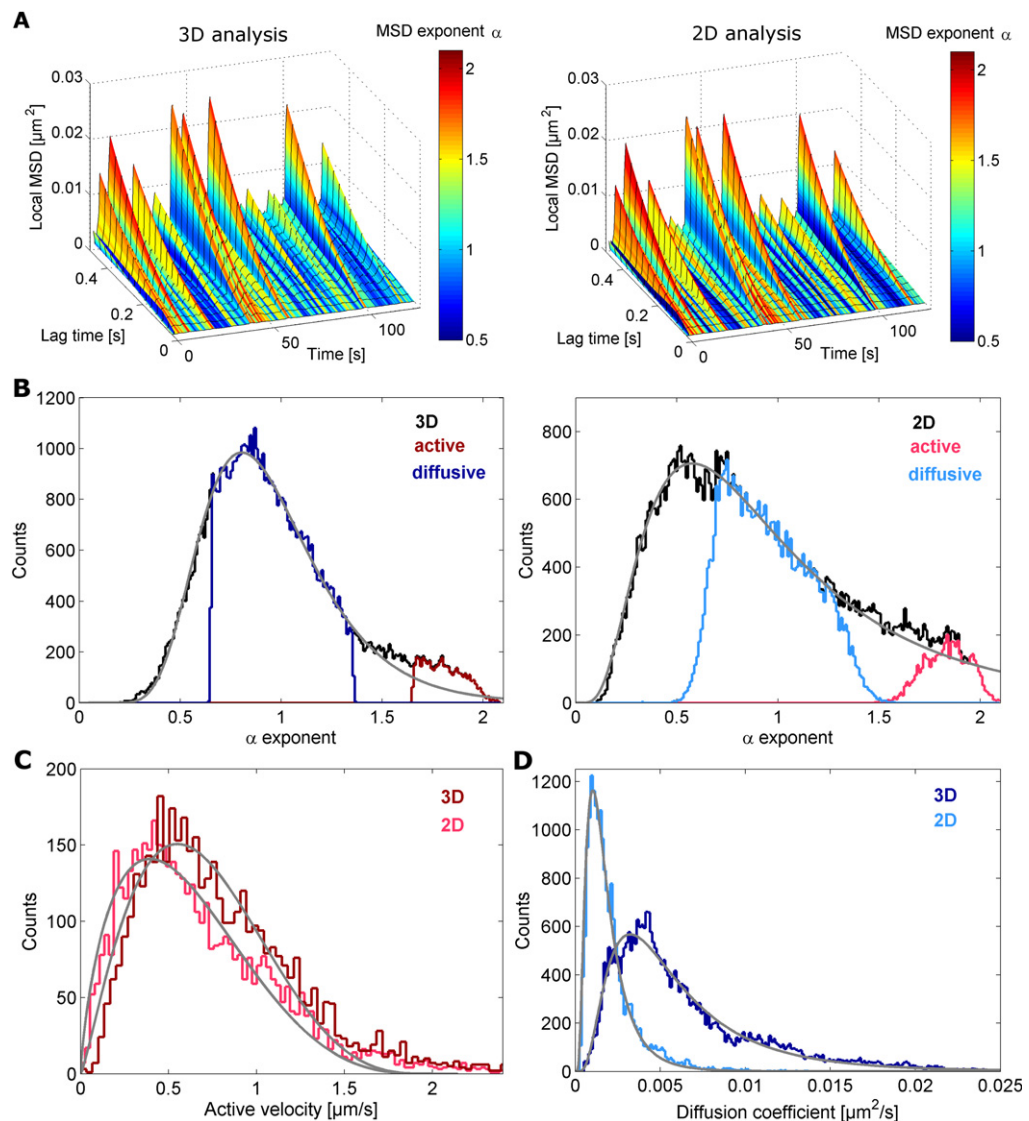
Figure 4. Comparison of the 3D and 2D *x–y* projection analyses in HuH-7 cells. (A) TRAnSpORT MSD plots from the 3D (left) and 2D (right) analyses of a nanoparticle moving within a HuH-7 cell. The general appearance is similar, the 2D MSD plot keeping all the features of the 3D analysis with similar magnitude. (B) Distributions of α-exponents obtained from the fit of the 3D (left) and 2D (right) MSDs for every time point. The distribution for active phases is shown in red and for passive phases in blue; the gray line is a fit to a lognormal distribution to guide the eye and to better extract the peak position for comparison. (C) Distributions of active transport velocities from the 3D analysis (dark red) and the 2D *x–y* projection (light red). The distributions were both fitted to a modified β function (gray line). (D) Distribution of diffusion coefficients during passive phases in 3D (dark blue) and in 2D (light blue) along with the respective fits to a lognormal distribution (gray line).

the data points, the distribution of the α-exponents was barely affected upon the 2D projection and analysis. In contrast, in the HuH-7 cells, where only 6% of the data points showed active transport, the distribution of the α-exponents obtained in the 2D analysis was broader than in 3D and the peak value was strongly reduced. In both cell types, the determination of the diffusion coefficient was biased by the 2D projection, leading to a value under-estimated by 33% for *D. discoideum* and by 69% for HuH-7 (see table 1). These values are significantly higher than what we measured for the diffusion coefficient of beads diffusing freely in a homogeneous solution of water and glucose, which was under-estimated by 18% in the 2D analysis. The diffusion was found to be faster in the ameba than in the human cells, the latter having a more complex and dense cytoskeleton that could hinder the free diffusion of particles in the cytoplasm. Indeed, the α-exponents and diffusion coefficients in the HuH-7 cells are significantly lower in 2D than in 3D and the confinement was more pronounced in the adherence plane than in the third dimension, suggesting an anisotropic organization of the intracellular structure of the HuH-7 cells. In *D. discoideum* cells where the cytoskeleton network is extended into the third dimension, a third of the active transport phases were incorrectly assigned to diffusive motion, whereas, in the quasi-2D cells (HuH-7), the identification and characterization of active transport was only barely affected by the 2D projection, confirming that the cytoskeleton network is mostly spread in the *x–y* plane and nearly all of the active transport takes place in this plane. In both cases, the determination of the velocity was not much affected, probably due to the previous selection of the active phases. The error in the diffusion coefficient determination together with the wrong α-exponent value (lower by 28%) illustrate that, although the HuH-7 cells are mostly spread in 2D, they cannot be considered as an isotropic milieu, at least with respect to diffusion. Therefore, a simple scaling from 2D to 3D is not possible. For the *D. discoideum* cells, there was no effect of the 2D projection on the α-exponent and the influence of the projection on the diffusion coefficient was less prominent. However, the active transport is evenly directed in 3D, causing misinterpretation and bias when transported particles are tracked in 2D only.

Restraining the analysis of a single-particle trajectory in live cells to its 2D projection limits the accuracy of the obtained values. More specific effects were revealed according to the cell shape and its extension along the third dimension. In general, the potential correction of these effects is not straightforward and cannot be obtained by a simple scaling. Hence, diffusion of particles on the cell membrane and active transport in flat cell lines such as HuH-7 may allow accurate analyses but, in general, additional work is necessary to understand and model the intracellular motion, to account for the observed effects and allow an accurate analysis of the 2D projected trajectory. The alternative is to acquire the live-cell trajectories directly in 3D; the analysis afterwards becomes more straightforward.

6. Conclusion

Herein we have investigated the consequences of analyzing the 2D projection of a single particle moving in 3D in living cells. After demonstrating the performances of our tracking instrument in 3D, we have shown the tracking of fluorescent nanoparticles in two types of cells: 3D roundish *D. discoideum* ameba and quasi-2D adherent human HuH-7 cells. The results of the 2D and 3D analyses with a local MSD algorithm on the 2D projection and the 3D trajectory, respectively, were then compared for both cell types. As expected from the 3D organization of the *D. discoideum* cytoskeleton, active transport along microtubules was performed isotropically in all

three directions. In contrast, the 2D projection of the active transport phases in the HuH-7 cells did not significantly alter the results, confirming the close to 2D organization of the cytoskeleton. However, the diffusion coefficients obtained with the 2D analysis were dramatically underestimated in both cell types, revealing that the intracellular diffusion is an anisotropic and complex process. Therefore, when accurate recognition of the types of motional behavior is desired and the results are to be analyzed quantitatively, it is necessary to track and analyze single particles in 3D.

Acknowledgments

References

[1] Lee G M, Ishihara A and Jacobson K A 1991 Direct observation of Brownian motion of lipids in a membrane *Proc. Natl Acad. Sci. USA* **88** 6274–8

[2] Courty S, Luccardini C, Bellaiche Y, Cappello G and Dahan M 2006 Tracking individual kinesin motors in living cells using single quantum-dot imaging *Nano Lett.* **6** 1491–5

[3] Gelles J, Schnapp B J and Sheetz M P 1988 Tracking kinesin-driven movements with nanometre-scale precision *Nature* **331** 450–3

[4] Saxton M J and Jacobson K 1997 Single-particle tracking: applications to membrane dynamics *Annu. Rev. Biophys. Biomol. Struct.* **26** 373–99

[5] Lange S *et al* 2008 Simultaneous transport of different localized mRNA species revealed by live-cell imaging *Traffic* **9** 1256–67

[6] Schutz G J, Kada G, Pastushenko V P and Schindler H 2000 Properties of lipid microdomains in a muscle cell membrane visualized by single molecule microscopy *EMBO J.* **19** 892–901

[7] Fujiwara T, Ritchie K, Murakoshi H, Jacobson K and Kusumi A 2002 Phospholipids undergo hop diffusion in compartmentalized cell membrane *J. Cell Biol.* **157** 1071–81

[8] Barak L S and Webb W W 1982 Diffusion of low density lipoprotein-receptor complex on human fibroblasts *J. Cell Biol.* **95** 846–52

[9] Kusumi A, Sako Y and Yamamoto M 1993 Confined lateral diffusion of membrane receptors as studied by single-particle tracking (nanovid microscopy). Effects of calcium-induced differentiation in cultured epithelial cells *Biophys. J.* **65** 2021–40

[10] Levi V, Ruan Q, Kis-Petikova K and Gratton E 2003 Scanning FCS: a novel method for three-dimensional particle tracking *Biochem. Soc. Trans.* **31** 997–1000

[11] Cang H, Xu C S, Montiel D and Yang H 2007 Guiding a confocal microscope by single fluorescent nanoparticles *Opt. Lett.* **32** 2729–31

[12] Dupont A and Lamb D C 2011 Nanoscale three-dimensional single-particle tracking *Nanoscale* **3** 4532–41

[13] Lessard G A, Goodwin P M and Werner J H 2007 Three-dimensional tracking of individual quantum dots *Appl. Phys. Lett.* **91** 224106

IOP Institute of Physics Φ DEUTSCHE PHYSIKALISCHE GESELLSCHAFT

[14] Katayama Y, Burkacky O, Meyer M, Brauchle C, Gratton E and Lamb D C 2009 Real-time nanomicroscopy via three-dimensional single-particle tracking *ChemPhysChem.* **10** 2458–64

[15] Bouzigues C and Dahan M 2007 Transient directed motions of GABA(A) receptors in growth cones detected by a speed correlation index *Biophys J.* **92** 654–60

[16] Thompson M A, Casolari J M, Badieirostami M, Brown P O and Moerner W E 2010 Three-dimensional tracking of single mRNA particles in *Saccharomyces cerevisiae* using a double-helix point spread function *Proc. Natl Acad. Sci. USA* **107** 17864–71

[17] Montiel D, Cang H and Yang H 2006 Quantitative characterization of changes in dynamical behavior for single-particle tracking studies *J. Phys. Chem.* B **110** 19763–70

[18] Arcizet D, Meier B, Sackmann E, Rädler J O and Heinrich D 2008 Temporal analysis of active and passive transport in living cells *Phys. Rev. Lett.* **101** 248103

[19] Nandi A, Heinrich D and Lindner B 2012 Distributions of diffusion measures from a local mean-square displacement analysis *Phys. Rev.* E **86** 021926

[20] de Bruin K *et al* 2007 Cellular dynamics of EGF receptor-targeted synthetic viruses *Mol. Therapy* **15** 1297–305

[21] Neujahr R *et al* 1998 Microtubule-mediated centrosome motility and the positioning of cleavage furrows in multinucleate myosin II-null cells *J. Cell Sci.* **111** 1227–40

[22] von Gersdorff K, Ogris M and Wagner E 2005 Cryoconserved shielded and EGF receptor targeted DNA polyplexes: cellular mechanisms *Eur. J. Pharm. Biopharm.* **60** 279–85

[23] Qian H, Sheetz M P and Elson E L 1991 Single-particle tracking analysis of diffusion and flow in two-dimensional systems *Biophys. J.* **60** 910–21

[24] Otten M, Nandi A, Arcizet D, Gorelashvili M, Lindner B and Heinrich D 2012 Local motion analysis reveals impact of the dynamic cytoskeleton on intracellular subdiffusion *Biophys. J.* **102** 758–67